Supporting Information

**A Biosensor Material with Mechanically Robust, Fatigue-Resistance, Biocompatibility, Biodegradability, and Anti-Freezing Capabilities**

Yanqiang Wei,[a,b] Shuaicheng Jiang,[a,b] Jiongjiong Li,[a,b] Xiaona Li,[a,b] Kuang Li,[a,b] Jianzhang Li, ,[a,c],* and Zhen Fang[a,d,e],*

[a]Jiangsu Key Open Laboratory of Wood Processing and Wood-based Panel Technology, Nanjing Forestry University, No.159 Longpan Road, Nanjing 210037, China.

[b]College of Materials Science and Engineering, Nanjing Forestry University, No.159 Longpan Road, Nanjing 210037, China.

[c]MOE Key Laboratory of Wooden Material Science and Application, Beijing Forestry University, No.35 Tsinghua East Road, Beijing 100083, China.

[d]Department of Biochemistry & Molecular Biology, Michigan State University, No.603 Wilson Road, East Lansing, Michigan 48824, United States.

[e]Great Lakes Bioenergy Research Center- Michigan State University, 1129 Farm Lane, East Lansing, Michigan 48824, United States.

*Corresponding authors

E-mail address: lijzh@bjfu.edu.cn (J. Z. Li)

E-mail address: fangzhe8@msu.edu (Z.Fang)

**Experimental**

*Materials.* Soy protein isolate (SPI, 95% protein content) was obtained from Yuwang Ecological Food Industry Co., Ltd. (Shandong, China). Hydrogen peroxide (30 wt%), glycerol (GL, AR), polyethylene glycol-200 (PEG-200, AR), and sodium hydroxide (NaOH, AR) were supplied by Nanjing Chemical Reagents Co., Ltd. (Nanjing, China). $BaTiO_3$ (BT, 99% purity) and other chemicals were supplied by Aladdin Biochem Co., Ltd. (Shanghai, China). All chemicals were used without further purification. Deionized water was used for all experiments.

*Preparation of BT@Ag particles.* The BT@Ag hybrid particles were prepared by electroless plating to deposit Ag nanoparticles on the surface of BT.[1] Prior to the electroless plating, the BT nanoparticles were firstly sensitized with $SnCl_2$ acidic solution. And then the depositing process was taken in the Rochelle salt plating bath, which is a mixture of bath A and bath B in accordance with practice. In consideration of the better dispersion of BT in ethanol and the electroless plating of silver in protonic solvent, both of the two bathes solvent were chosen as $H_2O$/ethanol (v/v = 8: 2), instead of $H_2O$ only. Taking the theoretical calculated mass ratio of BT/Ag = 90/10 for example, 3 g BT was dispersed in bath A with 10 ml of 0.2 M silver ammonia solution, following by low-speed agitation and ultrasonic treatment for 30 min. Afterward equal volume of bath B was added to the brown dispersion with high-speed agitation constantly, bath B involved 0.7 M of potassium sodium tartrate and 0.9 M of $MgSO_4$ in the mixed solvent. After reacting 2 h at room temperature, the dark brown dispersion was centrifuged at 4000 rpm for 15 min. The precipitate was washed three times with $H_2O$/ethanol by centrifugation. After drying the precipitate under vacuum at 60 °C for 4 h, strong brown powder, namely, BT@Ag was obtained. The collected BT@Ag particles was stored at 4 °C before usage.

*Preparation of SPI-based film.* The SPI-based film was prepared by a solution casting method.[2] Firstly, SPI powder (5 g) was added to distilled water (95 g) and the mixture was stirred vigorously for 1 h at 60 °C. Then, GL and PEG-200 were dispersed into the above solution and

stirring was continued for 30 min. The pH of the solution was adjusted to $9.0 \pm 0.1$ with 1 M NaOH. BT or BT@Ag (0.1-0.5 wt%, based on the above solution) was incorporated in the above solution and the resulting mixture was sonicated for 30 min. Finally, the resultant solution was poured into Teflon-coated plates and vacuum-dried at 45 °C for 48 h. The film materials were then peeled off and stored in a desiccator (25 °C and 50% relative humidity) for subsequent testing.

*Characterization of SPI-based films.* Attenuated total reflection Fourier transform infrared spectroscopy (ATR-FTIR) was obtained from a Nicolet iS50 infrared spectrophotometer (Thermo Fisher Scientific Co., Ltd, USA) in the range from 400 $cm^{-1}$ to 4000 $cm^{-1}$ with a resolution of 4 $cm^{-1}$ at ambient temperature for 32 scans. Chemical structure analysis of SPI-based film was performed using the X-ray photoelectron spectroscopy (XPS, AXIS UltraDLD, Britain) and X-ray diffraction patterns (XRD, Ultima IV analyzer, Rigaku, Japan). Thermogravimetric (TG) analysis was conducted using a thermal analyzer (TGA55, TA Instruments, USA) scanned from 30 °C to 800 °C at a heating rate of 10 °C·$min^{-1}$ in a nitrogen atmosphere. A scanning electron microscope (SEM, Quanta 200, USA) and the energy dispersive spectrometer (EDS) were used to observe the microstructure of the film fracture after tensile failure.

*Mechanical testing.* The mechanical testing of the film samples was conducted using an electron universal testing machine (Shimadzu, AGS-X, Japan). Film samples with dimensions of 10 mm × 80 mm (width × length) were tested at a tensile speed of 20 mm·$min^{-1}$. Five replicates were used for each sample. The dynamic mechanical behavior of the films was analyzed using a dynamic thermomechanical analyzer (DMA, Q850, TA Instruments, USA). The film samples were tested from 20 to 180 °C with a constant frequency of 1 Hz at a heating rate of 5 °C $min^{-1}$.

*Rheology testing:* Rheology tests were conducted on an RST-CPS rheometer. Frequency sweep tests were performed within the parallel plates of 50 mm in diameter in the frequency range of $10^{-2}$ -$10^3$ rad/s at the strain amplitude of 1.0% at 25 °C.

*Folding fatigue-resistant property measurements:* The folding fatigue-resistant performance of the composites was evaluated using an MIT folding tester (Shenzhen PuYu Electronic Co. Ltd, Shenzhen, China). The samples were conditioned (50 ± 2% relative humidity, 25 ± 2 °C) in a desiccator for 48 h before tests. Film samples with dimensions of 10 mm × 80 mm (width × length) were tested at a folding speed of 200 times·$min^{-1}$. The thickness of the films was determined with a digimatic micrometer. The result for each sample was recorded by testing specimens in quintuplicate.

*Electrical performance.* The conductivity ($\delta$) of the samples was tested using a four-point probes resistivity measurement system (RTS-9, China) at 25 °C. Ten replicates were used for each group and the average was taken. The electrochemical properties of the SPI-based films were measured using a three-electrode configuration in a CHI760E electrochemical workstation (CH Instruments, USA). The film samples were tested in a 0.1 M phosphate buffer saline (PBS) electrolyte at 25 °C. Cyclic voltammetry was recorded from -1.0 V to 1.0 V at a rate of 100 mV·$s^{-1}$. The motion-sensing experiment was conducted using the developed SPI-based film (5 cm x 1 cm), attaching directly to a moving human body with conductive adhesive tapes, then the movement was monitored by the electrochemical workstation. During the test, the digital thermometer (DTM-280) was used to monitor the temperature in real time. The thickness of the films was determined with a digimatic micrometer.

*Cryogenic tolerance of the films.* The conductivity ($\delta$) of the samples was tested using a four-point probes resistivity measurement system (RTS-9, China) at -30 °C. Ten replicates were used for each group and the average was taken. The electrochemical properties of the SPI-based

films were measured using a three-electrode configuration in a CHI760E electrochemical workstation (CH Instruments, USA). The motion-sensing experiment was conducted using the developed SPI-based film (5 cm x 1 cm), attaching directly to a moving toy doll with conductive adhesive tapes at -30 °C, then the movement was monitored by the electrochemical workstation. During the test, the digital thermometer (DTM-280) was used to monitor the temperature in real time. The thickness of the films was determined with a digimatic micrometer.

*In vitro degradation assessment. In vitro* degradation experiments were carried out in a simulated physiological environment. Briefly, 100 mg of samples was placed in a conical flask containing 10 mL of PBS buffer. The conical flasks were placed in a shaker with the water bath (37 °C) at 60 rpm shaking speed. The degradation was recorded every 24 hours by photographing the conical flask.

*Cytocompatibility Analysis.* The cytocompatibility of the composite samples to L929 cells was evaluated using the MTT (methylthiazolyldiphenyl-tetrazolium bromide) colorimetric method. The L929 cells in logarithmic growth phase were counted and the cell concentration was adjusted. The cells were inoculated into 96 well plates at a concentration of $4 \times 10^3$ cells·mL$^{-1}$ in an atmosphere of 5% $CO_2$ and cultured in a constant temperature incubator (37 °C) for 24 hours. Under an inverted microscope, the cell morphology of each treatment group was examined. The medium containing in the sample was removed. Each well was cleaned three times using the 100 μ L·well$^{-1}$ of PBS, then 100 μ L·well$^{-1}$ of medium containing 0.5 mg·mL$^{-1}$ of MTT and 5% $CO_2$ was added and incubated in the constant temperature incubator (37 °C) for 4 hours. The supernatant was then discarded and 100 μ L·well$^{-1}$ of dimethyl sulfoxide (DMSO) was added. After shaking for 10 minutes, the absorbance at 570 nm was detected.

*Biodegradable performance.* The oven-dried film materials (20 mm × 20 mm, width × length) were wrapped by plastic mesh and immersed in the soil inoculation source. Finally, the films

were weighted every 7 days and the weight residue was calculated based on the weight ratio between the degraded film and the original film.

**Results and Discussion**
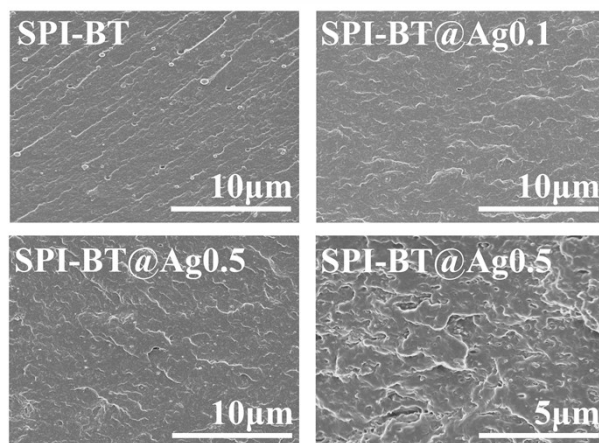


**Figure 4.** SEM images of SPI-based films.

**Table S1.** Mechanical properties of SPI-based films.

| Samples | Strain at break [%] | Yield strength [MPa] | Toughness [MJ·m$^{-3}$] |
|---|---|---|---|
| SPI-BT0.1 | 51.2 | 9.0 | 4.14 |
| SPI-BT@Ag0.1 | 117.7 | 14.2 | 15.4 |
| SPI-BT@Ag0.2 | 94.1 | 19.3 | 17.4 |
| SPI-BT@Ag0.3 | 88.3 | 24 | 18.1 |
| SPI-BT@Ag0.5 | 57.8 | 37.6 | 19 |

**Table S2**. Tensile strength of SPI-BT@Ag0.5 and other nanocomposite materials.

| Samples | Composites | Strain at break [%] | Yield strength [MPa] | Refs |
|---|---|---|---|---|
| 1 | TA@CNF | 11.6 | 16 | 3 |
| 2 | Rapeseed oil | 4.2 | 1.9 | 4 |
| 3 | Agar | 38.89 | 13.62 | 5 |
| 4 | Chitosan | 30.8 | 5.0 | 6 |
| 5 | ZnO nanorod | 12.64 | 14.74 | 7 |
| 6 | SPI/MMT | 5 | 8.5 | 8 |
| 7 | ASP/CMC | 20 | 5.97 | 9 |
| 8 | Lignocellulosic | 4.40 | 38.3 | 10 |
| 9 | Starch/AEEP | 40 | 21.6 | 11 |
| 10 | PS/BNNS | 3.5 | 37.8 | 12 |
| 11 | BN/PVA | 2.5 | 30 | 13 |
| 12 | PVA/BNNS | 28 | 5.2 | 14 |
| 13 | CNF/BNNS | 2 | 38.8 | 15 |
| 14 | MTM/PVA-PVAm | 40.8 | 21.0 | 16 |
| 15 | LAP/PVA | 22.0 | 12.5 | 17 |
| 16 | RGO/PDA | 5 | 4 | 18 |
| 17 | RGO/CS | 10.4 | 17.7 | 19 |
| 18 | RGO/MoS2-TPU | 5.8 | 6.9 | 20 |
| 19 | RGO/CS-Cu+ | 4.4 | 14.0 | 21 |
| 20 | SPI-BN | 13.3 | 36.4 | 22 |
| 21 | VPVA–HA | 59.7 | 55.6 | 23 |
| 22 | SPI-HBT0.25-GL0.5 | 111.50 | 12.18 | 2 |
| 23 | SPI-BT@Ag0.5 | 57.8 | 37.6 | This work |

**Table S3.** Toughness and strain of SPI-BT@Ag0.5 and other nanocomposite materials.

| Samples | Composites | Strain at break [%] | Toughness [MJ·m$^{-3}$] | Refs |
|---|---|---|---|---|
| 1 | MTM/PVA | 1.7 | 2.1 | 24 |
| 2 | TA@CNF/SPI-BNNS | 11 | 1.87 | 3 |
| 3 | LAP/PVA | 22.0 | 12.5 | 17 |
| 4 | RGO/PVA | 10.4 | 8.5 | 25 |
| 5 | RGO/PAPB | 4.3 | 7.5 | 26 |
| 6 | GO/PDA-UPy | 5.3 | 11.1 | 27 |
| 7 | GO/PAA | 7.9 | 8.9 | 28 |
| 8 | MTM/NFC | 2.8 | 2.3 | 29 |
| 9 | RGO/CS | 10.4 | 17.7 | 19 |
| 10 | MXene/NFC | 16.7 | 14.8 | 30 |
| 11 | SPI-BN | 13.3 | 2.58 | 22 |
| 12 | MTM/PVA-PVAm 50/50 | 40.8 | 21.0 | 16 |
| 13 | PVA/LA-10 | 129 | 80.4 | 31 |
| 14 | SPI-BT@Ag0.5 | 57.8 | 21.8 | This work |

**Table S4.** Comparison of conductivity of SPI-BT@Ag0.5 film with other nanocomposite materials in previous studies.

| Samples | Composites | Yield strength [MPa] | Conductivity [S·m$^{-1}$] | Refs |
|---|---|---|---|---|
| 1 | PLLA/SPFG | 34.1 | $5.62 \times 10^{-5}$ | 32 |
| 2 | PLLA/SPFG | 47.8 | 0.96 | 32 |
| 3 | PANB/SIS/RGO | <2.5 | $7.70 \times 10^{-2}$ | 33 |
| 4 | PVDF/PDA@BT | 40 | $5.51 \times 10^{-5}$ | 34 |
| 5 | PETMP/PEGDA/MOFs | 9.4 | $2.26 \times 10^{-2}$ | 35 |
| 6 | Silk/Laponite | ≤34 | 0.17 | 36 |
| 7 | Starch/MWCNTs | 9.8 | $0.04 \times 10^{-1}$ | 37 |
| 8 | ELO/PANI/CNT | 42.51 | $4.53 \times 10^{-3}$ | 38 |
| 9 | SPI/TPy@CNF | 14.5 | 0.078 | 39 |
| 10 | SPI/HPPy@CNF | 13.4 | $1.00 \times 10^{-4}$ | 40 |
| 11 | SPI/RGO/SNC | 10.2 | $6.58 \times 10^{-2}$ | 41 |
| 12 | SPI/CNC-CHO | 10.9 | $5.88 \times 10^{-4}$ | 42 |
| 13 | SPI/PA/CNF@Py-3 | 13.69 | $8.15 \times 10^{-6}$ | 43 |
| 14 | SPI-BT@Ag0.5-1000 times | 38 | 6.12 | This work |
| 15 | SPI-BT@Ag0.5-5000 times | 37.1 | 6.0 | This work |
| 16 | SPI-BT@Ag0.5-10000 times | 34.1 | 5.8 | This work |
| 17 | SPI-BT@Ag0.5-20000 times | 29.5 | 3.97 | This work |
| 18 | SPI-BT@Ag0.5-30000 times | 22 | 1.73 | This work |
| 19 | SPI-BT@Ag0.5 | 37.6 | 6.25 | This work |

References

1. L. Ren, X. Meng, J.-W. Zha, Z.-M. Dang, *RSC Adv.*, 2015, **5**, 65167-65174.
2. Y. Wei, S. Jiang, X. Li, J. Li, Y. Dong, S. Q. Shi, J. Li, Z. Fang, *ACS Appl. Mater. Interfaces*, 2021, **13**, 37617-37627.
3. Z. Wang, Y. Wen, S. Zhao, W. Zhang, Y. Ji, S. Zhang, J. Li, *Ind. Crop. Prod.*, 2019, **137**, 239-247.
4. K. Li, S. Jin, H. Chen, J. He, J. Li, *Polymers*, 2017, **9**, 167.
5. S. Mohajer, M. Rezaei, S. F. Hosseini, *Carbohydr. Polym.*, 2017, **157**, 784-793.
6. K. Li, S. Jin, X. Liu, H. Chen, J. He, J. Li, *Polymers*, 2017, **9**, 247.
7. Z. Wang, S. Zhao, A. Huang, S. Zhang, J. Li, *Carbohydr. Polym.*, 2019, **205**, 72-82.
8. I. Echeverria, P. Eisenberg, A. N. Mauri, *J. Membr. Sci.*, 2014, **449**, 15-26.
9. I. Choi, Y. Chang, S.-H. Shin, E. Joo, H. J. Song, H. Eom, J. Han, *Int. J. Mol. Sci.*, 2017, **18**, 1278.
10. M. Chen, X. Zhang, C. Liu, R. Sun, F. Lu, *ACS Sustain. Chem. Eng.*, 2014, **2**, 1164-1168.
11. Z. Soeyler, M. A. R. Meier, *Green Chem.*, 2017, **19**, 3899-3907.
12. X. Wang, P. Wu, *ACS Appl. Mater. Interfaces*, 2017, **9**, 19934-19944.
13. J. Wang, Y. Wu, Y. Xue, D. Liu, X. Wang, X. Hu, Y. Bando, W. Lei, *J. Mater. Chem. C*, 2018, **6**, 1363-1369.
14. J. Chen, H. Wei, H. Bao, P. Jiang, X. Huang, *ACS Appl. Mater. Interfaces*, 2019, **11**, 31402-31410.
15. K. Wu, J. Fang, J. Ma, R. Huang, S. Chai, F. Chen, Q. Fu, *ACS Appl. Mater. Interfaces*, 2017, **9**, 30035-30045.
16. A. Eckert, T. Rudolph, J. Guo, T. Mang, A. Walther, *Adv. Mater.*, 2018, **30**, 1802477.
17. P. Das, J.-M. Malho, K. Rahimi, F. H. Schacher, B. Wang, D. E. Demco, A. Walther, *Nat. Commun.*, 2015, **6**, 5967.
18. W. Cui, M. Li, J. Liu, B. Wang, C. Zhang, L. Jiang, Q. Cheng, *ACS Nano*, 2014, **8**, 9511-9517.
19. S. Wan, J. Peng, Y. Li, H. Hu, L. Jiang, Q. Cheng, *ACS Nano*, 2015, **9**, 9830-9836.
20. S. Wan, Y. Li, J. Peng, H. Hu, Q. Cheng, L. Jiang, *ACS Nano*, 2015, **9**, 708-714.
21. Y. Cheng, J. Peng, H. Xu, Q. Cheng, *Adv. Funct. Mater.*, 2018, **28**, 1800924.
22. S. Jiang, Y. Wei, S. Q. Shi, Y. Dong, C. Xia, D. Tian, J. Luo, J. Li, Z. Fang, *Nano Lett.*, 2021, **21**, 3254-3261.
23. Y. Li, S. Li and J. Sun, *Adv. Mater.*, 2021, **33**, 2007371.
24. A. Walther, I. Bjurhager, J.-M. Malho, J. Pere, J. Ruokolainen, L. A. Berglund, O. Ikkala, *Nano Lett.*, 2010, **10**, 2742-2748.
25. N. Zhao, M. Yang, Q. Zhao, W. Gao, T. Xie, H. Bai, *ACS Nano*, 2017, **11**, 4777-4784.
26. M. Zhang, L. Huang, J. Chen, C. Li, G. Shi, *Adv. Mater.*, 2014, **26**, 7588-7592.
27. Y. Wang, T. Li, P. Ma, S. Zhang, H. Zhang, M. Du, Y. Xie, M. Chen, W. Dong, W. Ming, *ACS Nano*, 2018, **12**, 6228-6235.
28. S. Wan, H. Hu, J. Peng, Y. Li, Y. Fan, L. Jiang, Q. Cheng, *Nanoscale*, 2016, **8**, 5649-5656.
29. A. Liu, A. Walther, O. Ikkala, L. Belova, L. A. Berglund, *Biomacromolecules*, 2011, **12**, 633-641.
30. W.-T. Cao, F.-F. Chen, Y.-J. Zhu, Y.-G. Zhang, Y.-Y. Jiang, M.-G. Ma, F. Chen, *ACS Nano*, 2018, **12**, 4583-4593.
31. X. Zhang, W. Liu, D. Yang and X. Qiu, *Adv. Funct. Mater.*, 2019, **29**, 1806912.
32. C.-C. Cheng, Z.-S. Liao, J.-J. Huang, S.-Y. Huang, W.-L. Fan, *Compos. Sci. Technol.*, 2017, **148**, 89-96.

33. S. Mazhar, B. P. Lawson, B. D. Stein, M. Pink, J. Carini, A. Polezhaev, E. Vlasov, S. Zulfiqar, M. I. Sarwar, L. M. Bronstein, *J. Polym. Res.*, 2020, **27,** 105.
34. Y. Xie, Y. Yu, Y. Feng, W. Jiang, Z. Zhang, *ACS Appl. Mater. Interfaces*, 2017, **9**, 2995-3005.
35. H. Wang, Q. Wang, X. Cao, Y. He, K. Wu, J. Yang, H. Zhou, W. Liu, X. Sun, *Adv. Mater.*, 2020, **32**, e2001259.
36. F. B. Kadumudi, M. Jahanshahi, M. Mehrali, T. G. Zsurzsan, N. Taebnia, M. Hasany, S. Mohanty, A. Knott, B. Godau, M. Akbari, A. Dolatshahi-Pirouz, *Adv. Sci.*, 2019, **6**, 1801241.
37. D. Domene-Lopez, J. J. Delgado-Marin, J. C. Garcia-Quesada, I. Martin-Gullon, M. G. Montalban, *Carbohydr. Polym.*, 2020, **229**, 115545.
38. V. Khandelwal, S. K. Sahoo, A. Kumar, S. K. Sethi, G. Manik, *Compos. Part B-Eng.*, 2019, **172**, 76-82.
39. Z. Wang, S. Zhao, A. Huang, S. Zhang, J. Li, *Carbohydr. Polym.*, 2019, **205**, 72-82.
40. S. Jin, K. Li, Q. Gao, W. Zhang, H. Chen, J. Li, *Carbohydr. Polym.*, 2020, **237**, 116141.
41. G. Zhu, A. Dufresne, N. Lin, *ACS Sustain. Chem. Eng.*, 2017, **5**, 9431-9440.
42. D.-Y. Xie, D. Qian, F. Song, X.-L. Wang, Y.-Z. Wang, *ACS Sustain. Chem. Eng.*, 2017, **5**, 7063-7070.
43. K. Li, S. Jin, X. Li, S. Q. Shi, J. Li, *J. Clean. Prod.*, 2021, **285**, 125504.